JGR Atmospheres

RESEARCH ARTICLE
10.1029/2019JD030396

Special Section:
Long-term Changes and Trends in the Middle and Upper Atmosphere

Interannual Variations in Lower Stratospheric Ozone During the Period 1984–2016

Jinpeng Lu[1], Fei Xie[1,2], Wenshou Tian[3], Jianping Li[1,2], Wuhu Feng[4,5], Martyn Chipperfield[5], Jiankai Zhang[3], and Xuan Ma[1]

[1]Change and Earth System Science, Beijing Normal University, Beijing, China, [2]Laboratory for Regional Oceanography and Numerical Modeling, Qingdao National Laboratory for Marine Science and Technology, Qingdao, China, [3]College of Atmospheric Sciences, Lanzhou University, Lanzhou, China, [4]National Centre for Atmospheric Science, University of Leeds, Leeds, UK, [5]School of Earth and Environment, University of Leeds, Leeds, UK

Abstract In this work we investigate interannual variations in lower stratospheric ozone from 1984 to 2016 based on a satellite-derived data set and simulations from a chemical transport model. An empirical orthogonal function (EOF) analysis of ozone variations between 2000 and 2016 indicates that the first, second, and third EOF modes are related to the quasi-biennial oscillation (QBO), canonical El Niño–Southern Oscillation (ENSO), and ENSO Modoki events, respectively; these three leading EOFs capture nearly 80% of the variance. However, for the period 1984–2000, the first, second, and third modes are related to the QBO, ENSO Modoki, and canonical ENSO events, respectively. The explained variance of the second mode in relation to ENSO Modoki is nearly twice that of the third mode for canonical ENSO. Since the frequency of ENSO Modoki events was higher from 1984 to 2000 than after 2000, the Brewer-Dobson circulation anomalies related to ENSO Modoki were stronger during 1984–2000, which caused ENSO Modoki events to have a greater effect on lower stratospheric ozone before 2000 than after. Ozone anomalies associated with QBO, ENSO Modoki, and canonical ENSO events are largely caused by dynamic processes, and the effect of chemical processes on ozone anomalies is opposite to that of dynamic processes. Ozone anomalies related to dynamic processes are 3–4 times greater than those related to chemical processes.

Key Points:
- The second and third EOFs of the interannual variations in lower stratospheric ozone during 2000-2016 are related to canonical ENSO and ENSO Modoki, respectively
- For the period 1984-2000, the second EOF is related to ENSO Modoki and the third EOF to canonical ENSO
- The higher frequency of occurrence of ENSO Modoki than canonical ENSO led to a stronger impact of ENSO Modoki on circulation and ozone anomalies between 1984 and 2000

Correspondence to:
F. Xie,
xiefei@bnu.edu.cn

Citation:
Lu, J., Xie, F., Tian, W., Li, J., Feng, W., Chipperfield, M., et al. (2019). Interannual variations in lower stratospheric ozone during the period 1984–2016. *Journal of Geophysical Research: Atmospheres*, *124*, 8225–8241. https://doi.org/10.1029/2019JD030396

Received 30 JAN 2019
Accepted 12 JUN 2019
Accepted article online 9 JUL 2019
Published online 29 JUL 2019

Author Contributions:
Conceptualization: Jinpeng Lu, Fei Xie
Data curation: Jinpeng Lu, Fei Xie
Formal analysis: Jinpeng Lu, Fei Xie
Funding acquisition: Fei Xie
Investigation: Jinpeng Lu, Fei Xie
Methodology: Jinpeng Lu, Fei Xie
Project administration: Fei Xie
Resources: Jinpeng Lu, Fei Xie
Software: Jinpeng Lu, Fei Xie
Supervision: Fei Xie
Validation: Jinpeng Lu, Fei Xie
Visualization: Jinpeng Lu, Fei Xie
(continued)

1. Introduction

Stratospheric ozone absorbs solar radiation in the ultraviolet range of light, thereby protecting life on Earth (e.g., Kerr & McElroy, 1993; Lubin & Jensen, 1995) and affecting atmospheric temperature via radiative heating (e.g., Forster et al., 1997; Haigh, 1994; Ramaswamy et al., 1996; Tian et al., 2010). At the same time, radiative heating affects stratospheric circulation. Circulation anomalies can transport heat downwards and thereby influence troposphere weather and climate (e.g., Baldwin & Dunkerton, 2001; Cagnazzo et al., 2009; Graf & Walter, 2005; Ineson & Scaife, 2009; Karpechko et al., 2014; Kidston et al., 2015; Reichler et al., 2012; Son et al., 2008; Thompson et al., 2011; Wang et al., 2013; Wang et al., 2018; Xie et al., 2016; Zhang et al., 2016). Through these processes and interactions, stratospheric ozone has a profound impact on the climate system. Therefore, an understanding of ozone variability is still an active research topic.

WMO (World Meteorological Organization), Scientific Assessment of Ozone Depletion (2018) has reported that the upper stratospheric ozone has increased from 1995 to 2016. However, ozone in the lower stratosphere still showed a continuing declining trend (Ball et al., 2017, 2018; Gebhardt et al., 2014; Kyrölä et al., 2013; Nair et al., 2015; Sioris et al., 2014; Vigouroux et al., 2015; Zhang et al., 2018). In addition to trends, the interannual variations in lower stratospheric ozone also require detailed investigations, since the changes in lower stratospheric ozone can significantly influence climate change (Forster et al., 1997; Hu et al., 2015; Polvani et al., 2017). However, the interannual variations of lower stratospheric ozone and its relevant control factors for the period from 1995 to 2016 have not received enough attention. Moreover, a better understanding of the factors influencing interannual variations of ozone in the lower stratosphere will help us to accurately estimate the change of ozone in the future.

It is well-known that the El Niño–Southern Oscillation (ENSO) is one of the important processes controlling the interannual variations of stratospheric ozone by affecting the tropical stratospheric circulation (Fusco &

Writing - original draft: Jinpeng Lu, Fei Xie
Writing – review & editing: Jinpeng Lu, Fei Xie, Wenshou Tian, Jianping Li, Wuhu Feng

Salby, 1999). The enhanced tropical upwelling warms the upper troposphere and cools the lower stratosphere in the tropics during El Niño phases (Calvo et al., 2010; Free & Seidel, 2009; Garcia-Herrera et al., 2006; Randel et al., 2009), influencing coherent tropical ozone and water vapor (Fueglistaler & Haynes, 2005; Geller et al., 2002; Gettelman et al., 2001; Hatsushika & Yamazaki, 2003; Scaife et al., 2003; Xie et al., 2012). The Aleutian Low in the Pacific North American pattern deepens (e.g., Garcia-Herrera et al., 2006), and the vertical propagation of ultralong Rossby waves is intensified during El Niño activity in the Northern Hemisphere (NH) in winter. Observational data set shows anomalous increased wave dissipation in the stratosphere in the NH middle and high latitudes, warming Arctic stratosphere (Camp & Tung, 2007; Free & Seidel, 2009; Garfinkel & Hartmann, 2007, 2008; Ren et al., 2012; Van Loon & Labitzke, 1987; Wei et al., 2007) and cooling the equatorial stratosphere (Li et al., 2016), which were also supported by the simulations (Garcia-Herrera et al., 2006; Garfinkel et al., 2013; Hamilton, 1995; Manzini et al., 2006; Rao & Ren, 2016; Sassi et al., 2004; Taguchi & Hartmann, 2006; Xie et al., 2012). The enhanced Brewer-Dobson (BD) circulation is associated with the polar warming during El Niño events (Brewer, 1949), which transports more tropical ozone from the source regions to high polar latitudes. Both observations and simulations show that total column ozone (TCO) is accumulated at Arctic and midlatitude sites during El Niño events (Brönnimann et al., 2004, 2006; Cagnazzo et al., 2009). La Niña activity has the opposite effect on the middle latitude and polar stratosphere (Free & Seidel, 2009; Mitchell et al., 2011; Iza & Calvo, 2015; Iza et al., 2016; Zhang et al., 2015).

In recent decades, a change in the ENSO anomaly pattern, named the Central Pacific type (or ENSO Modoki), which is distinct from the familiar Eastern Pacific type (canonical ENSO), has been gradually discovered (Ashok & Yamagata, 2009; Yeh et al., 2009). The climatic effects of ENSO Modoki on stratospheric circulation and ozone are different from canonical ENSO because of the different spatial patterns of sea surface temperature (SST) anomalies (SSTAs) between the two events (Hegyi & Deng, 2011; Hurwitz, Newman, et al., 2011; Hurwitz, Song, et al., 2011; Iza & Calvo, 2015; Sung et al., 2014; Xie et al., 2012; Xie, Li, Tian, & Shu, 2014; Xie, Li, Tian, & Sun, 2014; Zubiaurre & Calvo, 2012).

In addition to ENSO, the quasi-biennial oscillation (QBO) also controls the interannual variations of stratospheric ozone. The QBO is a downward-propagating oscillating pattern of equatorial stratospheric winds and temperatures with a period of around 2 years. Reed (1964) found that the QBO would induce the meridional circulation and then drive a QBO signal in TCO. In the easterly phase, defined as a descending QBO, enhanced upwelling at the equator in the lower stratosphere would lead to a negative anomaly in column ozone. However, during the QBO westerly phase, there would be a positive column ozone anomaly caused by reversed circulation. Subsequently, the temporal and spatial characteristics of the QBO signal in stratospheric ozone have been analyzed, including the mechanism of how the QBO influences ozone. At the same time, a large number of related studies have been performed with observations and simulations (e.g., Butchart et al., 2003; Lee et al., 2010; Randel & Wu, 1996; Tian et al., 2006).

Although it is known that ENSO and the QBO affect the interannual variations in stratospheric ozone, the different contributions of these factors on lower stratospheric ozone changes in the period 2000–2016 is still unclear. Furthermore, it is also important to investigate whether the relative influences of these factors on ozone interannual variability are changing over time by comparing their contributions to ozone changes during this period with pre-2000. We address these issues in this work. The paper is organized as follows. Section 2 describes the observational and simulation data sets and our methods. In section 3, we show results for the different contributions of factors to lower stratospheric ozone variation. The relevant mechanisms for interannual variations in ozone are analyzed in section 4. Finally, we discuss the results and draw conclusions in section 5.

2. Data, Methods, and Models

Monthly mean ozone is taken from the Stratospheric Water and Ozone Satellite Homogenized (SWOOSH) data set, which is a merged record of stratospheric ozone and water vapor measurements taken by a number of limb sounding and solar occultation satellites over the period from 1984 to 2013 (Davis et al., 2016). Its primary product is a monthly mean zonal-mean gridded data set (2.5° from 89°S to 89°N) containing ozone and water vapor data from the SAGE-II/III, UARS HALOE, UARS

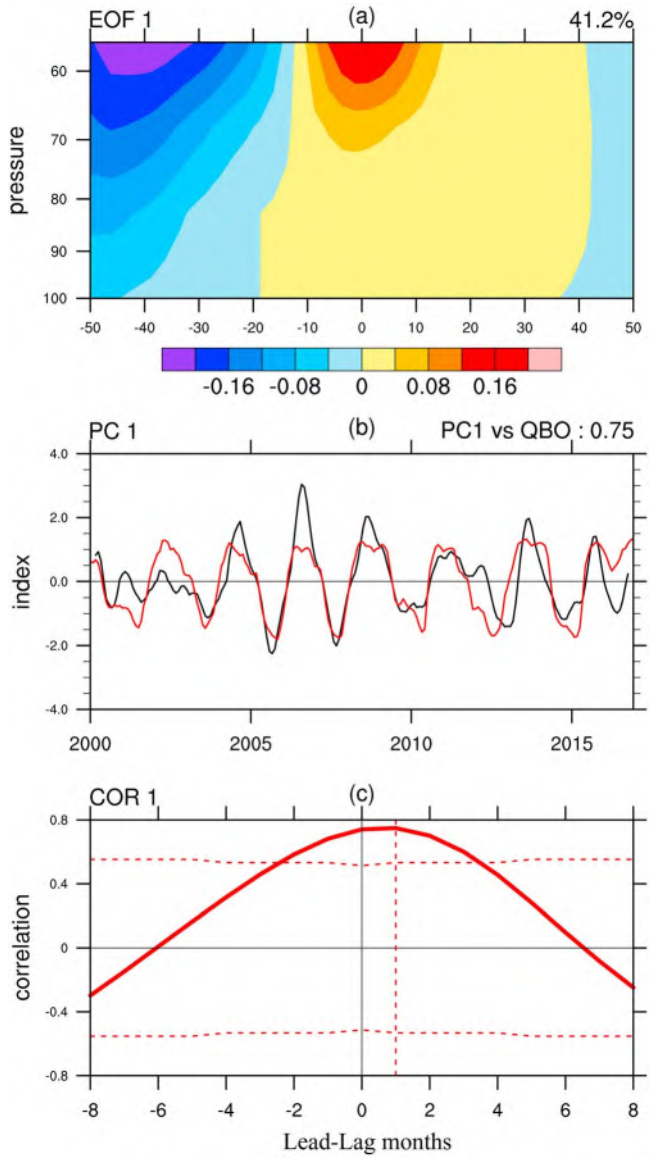

Figure 1. EOF analysis of zonal mean ozone variability for the period 2000–2016 based on Stratospheric Water and Ozone Satellite Homogenized data covering 50°S to 50°N and 100–50 hPa. Ozone anomalies were obtained by removing the annual cycle and linear trend from the original time series at each grid cell. The square root of the cosine of latitude was used for the weighting function in the EOF analysis. (a) The spatial pattern of the first EOF mode (EOF1). The value in the upper right corner is the explained variance of the mode. (b) The first principal component (PC1; black line) and the QBO index (red line). (c) Lead-lag correlation between PC1 and the QBO index for 2000–2016. Positive lead-lag values indicate that the QBO index leads PC1. The dotted lines denote the 95% confidence interval with statistical significance determined using the two-tailed Student's *t* test. EOF = empirical orthogonal function; PC = principal component; QBO = quasi-biennial oscillation.

MLS, and Aura MLS instruments. The vertical pressure range of the ozone data is 316–1 hPa (31 levels). For more information, see Davis et al. (2016).

The QBO index is defined as the zonal average of the 30-hPa zonal wind at the equator as computed from the NCEP/NCAR Reanalysis (Randel & Wu, 1996; Wallace et al., 1993). The zonal mean wind is less than −5 m/s in the easterly phase of the QBO and greater than 5 m/s in the westerly phase of the QBO. The monthly NINO3.4 and Modoki indices (hereafter EMI) are used to represent monthly characteristics of canonical ENSO events and ENSO Modoki events, respectively. The NINO3.4 index is defined as the area-mean SSTAs over the region (5°N to 5°S, 120–170°W) and is available at http://www.cpc.noaa.gov/data/indices/. A standardized NINO3.4 index greater than 1 standard deviation (STD) is defined as a canonical El Niño event, and an index less than −1 STD is defined as a canonical La Niña event.

The EMI was defined as follows (Ashok et al., 2007):

$$\mathrm{EMI} = [\mathrm{SSTA}]_{\mathrm{C}} - 0.5\times[\mathrm{SSTA}]_{\mathrm{E}} - 0.5\times[\mathrm{SSTA}]_{\mathrm{W}}.$$

Terms in the formula represent the area-mean SSTA. $[\mathrm{SSTA}]_{\mathrm{C}}$ is the mean over the central Pacific region (10°S to 10°N, 165°E to 140°W), $[\mathrm{SSTA}]_{\mathrm{E}}$ is over the eastern Pacific region (15°S to 5°N, 110–70°W), and $[\mathrm{SSTA}]_{\mathrm{W}}$ is over the western Pacific region (10°S to 20°N, 125–145°E). SSTs were obtained from the Met Office Hadley Center SST data set (www.metoffice.gov.uk/hadobs/index.html). A standardized EMI greater than 1 STD is defined as an El Niño Modoki event, and an EMI less than −1 STD is defined as a La Niña Modoki event.

Edmon et al. (1980) calculated the BD circulation in a pressure coordinate system:

$$\overline{v}^{*} = \overline{v} - \left[\overline{(v'\theta')}/\overline{\theta}_p\right]_p,$$

$$\overline{\omega}^{*} = \overline{\omega} + (a\cos\varphi)^{-1}\left[\cos\varphi\left(\overline{v'\theta'}/\overline{\theta}_p\right)\right]_{\varphi},$$

where θ is the potential temperature, a is the radius of the Earth, $\overline{v}$ is the mean meridional wind, and $\overline{\omega}$ is average vertical velocity. The subscripts p and φ represent derivatives with pressure p and latitude φ, respectively. The overbar denotes the zonal mean, and the prime denotes the deviations from the zonal mean value.

The following approximation (Xie, Li, Tian, Zhang, & Sun, 2014) determines the effective number (N^{eff}) of degrees of freedom (Bretherton et al., 1999) in this paper:

$$\frac{1}{N^{\mathrm{eff}}} \approx \frac{1}{N} + \frac{2}{N}\sum_{j=1}^{N}\frac{N-j}{N}\rho_{XX}(j)\rho_{YY}(j),$$

where N is the sample size and ρ_{XX} and ρ_{YY} are the autocorrelations of two sampled time series, X and Y, at time lag j, respectively.

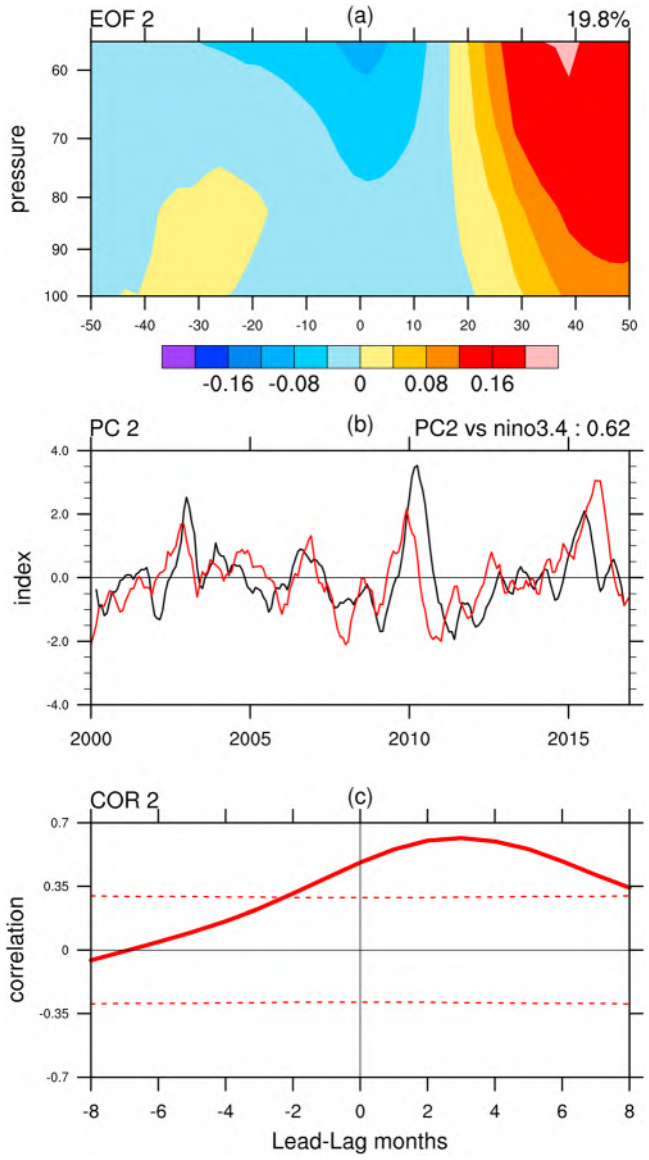

Figure 2. As in Figure 1 but for the second EOF mode and the NINO3.4 index (red line in b). EOF = empirical orthogonal function; PC = principal component.

We use the TOMCAT/SLIMCAT three-dimensional offline chemical transport model (Chipperfield, 2006) to perform EOF analyses and investigate the dynamic and chemical processes involved in ozone variability. The model has identical stratospheric chemistry and aerosol loading, solar flux input, and surface mixing ratios of long-lived source gases as Chipperfield et al. (2018). The model was run from 1979 to 2016. The model uses horizontal winds and temperature from the reanalysis data of the European Centre for Medium-Range Weather Forecasts (ECMWF)-Interim (Dee et al., 2011). Previous studies have found that the wind and temperature fields from the ECMWF-Interim reanalysis agree well with those from the Modern-Era Retrospective analysis for Research and Applications, version 2 (MERRA2), especially in middle and high latitudes (Lindsay et al., 2014; Rienecker et al., 2011). The long-term simulation (1979–2015) was performed with a coarse horizontal resolution of approximately 5.625° latitude × 5.625° longitude and 32 levels from the surface to 60 km. The model uses a hybrid $\sigma - p$ vertical coordinate (Chipperfield, 2006) with detailed tropospheric and stratospheric chemistry. Vertical advection is calculated from the divergence of the horizontal mass flux (Chipperfield, 2006), and chemical tracers are advected, conserving second-order moments (Prather, 1986). The TOMCAT/SLIMCAT model has been extensively evaluated against various ozone satellite and sounding data sets and provides a good representation of stratospheric chemistry (e.g., Chipperfield, 2006; Feng et al., 2007, 2011). The TOMCAT/SLIMCAT simulation initializes a "passive odd-oxygen" tracer that is set equal to the modeled chemical $O_x = O(^3P) + O(^1D) + O_3$ concentration on 1 December every year for the NH and then advected passively without chemistry. At any point after 1 December, the difference between this passive O_x and the model's chemically integrated O_x is the net chemical O_x change in air that has been advected to that point (Feng et al., 2005). O_x is mainly O_3 below 30 km, where the concentrations of O (^{3}P) and O (^{1}D) are small, especially in winter when there is no sunlight in the polar region. Hereafter, the passive O_x is referred to as "dynamic ozone," while the difference between the chemically integrated O_x and passive O_x is called "chemical ozone."

3. Factors Influencing the Interannual Variations in Lower Stratospheric Ozone

We first performed an EOF analysis of lower stratospheric ozone anomalies to investigate the EOF spatial patterns, principal components (PCs), and possible relevant impact factors of the corresponding three leading modes. We used SWOOSH data for the period 2000–2016, covering 50°S to 50°N and 100–50 hPa. Ozone anomalies were obtained by removing the annual cycle and linear trend from the original time series at each grid cell (not shown). The square root of the cosine of latitude was used for the weighting function in the EOF analysis. The first mode, which accounts for 41.2% of the variance, has a tripole pattern, that is, a positive phase of ozone in the tropical lower stratosphere at 20°S to 40°N and negative phases in the middle latitudes of both hemispheres at 50–20°S and at 40–50°N (Figure 1a). Note that the amplitude of ozone phase in the Southern Hemisphere (SH) is much larger than that in the NH. PC1 variations show a QBO signal (Figure 1b). When the QBO leads PC1 by 1 month, the correlation coefficient between PC1 and the QBO index is 0.75 and significant at the 95% confidence level (Figure 1c); the statistical significance of the correlation between the two autocorrelated time series was determined via a two-tailed Student's t test. This result suggests that the first mode is strongly related to the QBO. The pattern of the first EOF mode (Figure 1a) agrees with previous studies (e.g.,

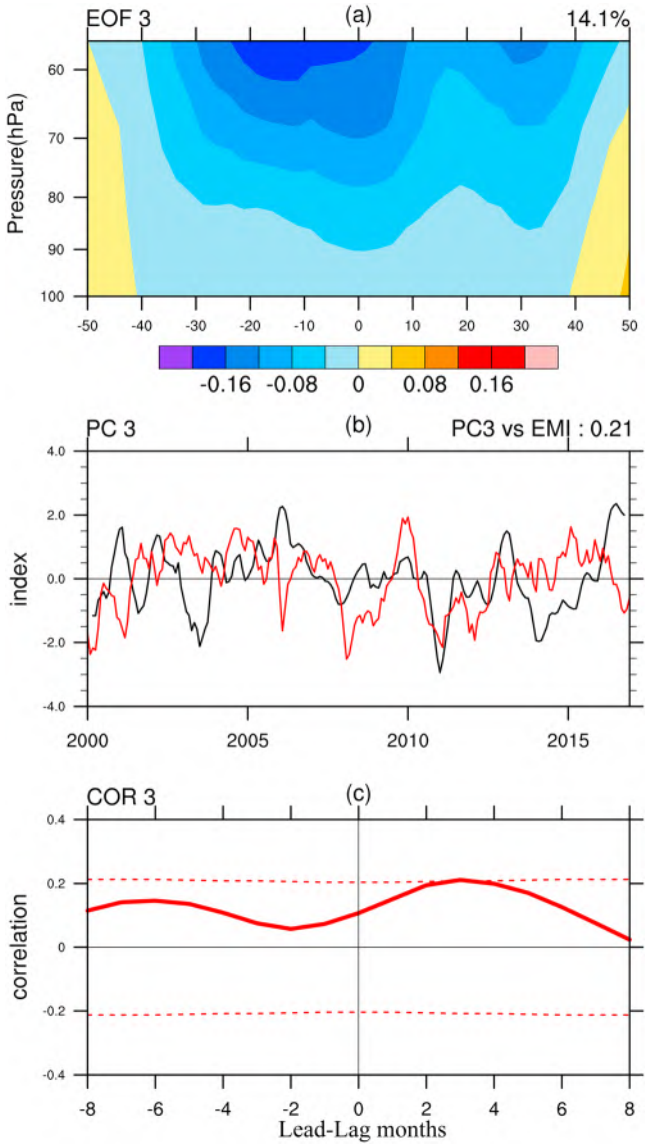

Figure 3. Same as in Figure 1 but for the third EOF mode and the El Niño–Southern Oscillation Modoki index (red line in b). EOF = empirical orthogonal function; EMI = El Niño–Southern Oscillation Modoki index; PC = principal component; QBO = quasi-biennial oscillation.

Table 1
Largest Lead-Lag Correlation Coefficients Between PC1/PC2/PC3 and QBO/NINO3.4/EMI Indices Based on 2000–2016 Stratospheric Water and Ozone Satellite Homogenized Data

	QBO	NINO3.4	EMI
PC1	0.75* (0.67, 0.80)	0.13 (−0.13, 0.15)	−0.20 (−0.32, −0.06)
PC2	−0.21 (−0.22, 0.08)	0.62* (0.37, 0.68)	0.39* (0.39, 0.59)
PC3	0.19 (−0.02, 0.25)	0.15 (0.04, 0.30)	0.21* (−0.03, 0.24)

Note. Asterisks indicate that the correlation coefficient is significant at the 95% confidence level. The values in brackets are the uncertainty range for the correlation coefficient at the 95% confidence level. EMI = El Niño–Southern Oscillation Modoki index; PC = principal component; QBO = quasi-biennial oscillation.

Randel & Wu, 1996) that investigated ozone anomalies associated with the QBO. The second EOF mode has a bipolar structure, that is, a negative phase of ozone in the tropical and SH lower stratosphere at 50°S–20°N and a positive phase in the NH at 20–50°N (Figure 2a). This mode accounts for 19.8% of the variance. PC2 is correlated with the NINO3.4 index (Figure 2b, $R = 0.62$), which leads PC2 variations by 3–4 months (Figure 2c). The pattern of the second EOF mode (Figure 2a) agrees with that of ozone anomalies caused by ENSO (e.g., Randel et al., 2009). The third EOF mode, which accounts for 14.1% of the variance, shows a relatively uniform change, that is, a negative ozone phase in the lower stratosphere at 40°S to 40°N and positive phases in the middle latitudes of both hemispheres at 50–40°S and at 40–50°N (Figure 3a). The correlation coefficient between PC3 and the ENSO Modoki index (EMI) is 0.21 when the EMI leads PC3 by 3 months (Figures 3b and 3c). The first three EOFs capture nearly 80% of the variance; therefore, the remaining modes only explain less amount of variance and will not be used for further analysis and discussions.

Table 1 provides the largest lead-lag correlation coefficients (R), together with their uncertainties, between the three leading PCs and the QBO index, the canonical ENSO index, and the EMI. For PC1, the correlation coefficient between PC1 and the QBO index is the largest; for PC2, the largest value of R is obtained with the NINO3.4 index; and for PC3, the largest R is between PC3 and the EMI. Note that there is a great deal of uncertainty (Table 1) in the correlation coefficients between PC2/PC3 and canonical ENSO/ENSO Modoki, since there is a correlative relationship between canonical ENSO and ENSO Modoki. To further check whether PC2 and PC3 are related respectively to canonical ENSO and ENSO Modoki, we compared the patterns of correlation coefficients between sea surface temperature anomalies and PC2/PC3 with SSTAs related to canonical ENSO and ENSO Modoki events. Figure 4 shows composite SSTAs associated with canonical ENSO and ENSO Modoki events during 2000–2016 (Figures 4a and 4b) and the spatial distribution of correlation coefficients between SSTAs and PC2/PC3 variations when the SSTAs lead PC2/PC3 by 3 months (Figures 4c and 4d). Table 2 shows spatial correlation coefficients (SRs) among Figures 4a, 4b, 4c, and 4d, together with their uncertainties. The pattern of canonical ENSO-related SSTAs (Figure 4a) is similar to the spatial distribution of correlation coefficients between SST and PC2 variations (Figure 4c). The corresponding SR between Figures 4a and 4c is 0.78 and significant at the 95% confidence level. Figure 4d shows that the distribution of correlation coefficients between SSTAs and PC3 variations is consistent with ENSO Modoki-related SSTAs (Figure 4b). The corresponding SR is 0.69 and significant at the 95% confidence level. Table 2 shows that the SR between Figures 4a and 4c is larger than that between Figures 4a and 4d, and the SR between Figures 4b and 4d is larger than that between Figures 4b and 4c. The spatial correlation further confirms that the PC2 of ozone changes during 2000–2016 is more possibly associated with canonical ENSO, and the third EOF mode is related to ENSO

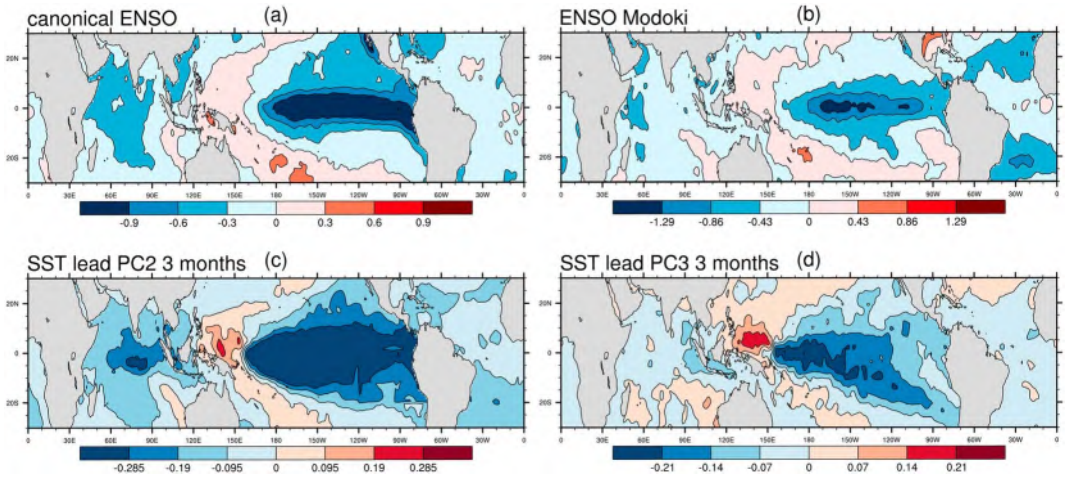

Figure 4. (a) Composite SST anomalies (multiplied by −1) associated with canonical ENSO events for the period 2000–2016. (b) As in (a) but for ENSO Modoki. (c) The spatial distribution of correlation coefficients between SST anomalies and PC2 variations when SST anomalies lead PC2 by 3 months. (d) As in (c) but for PC3. Details of canonical ENSO and ENSO Modoki events selected for composite analysis are given in Table 7. SST data are from the Hadley Center. ENSO = El Niño–Southern Oscillation; PC = principal component; SST = sea surface temperature.

Modoki. Note that the PC2 appears to be more correlated with canonical ENSO over the Indian Ocean but more correlated with ENSO Modoki over the Atlantic Ocean. PC3 is more correlated with ENSO Modoki over the Indian Ocean but more correlated with canonical ENSO over the Atlantic Ocean. This phenomenon deserves further investigation.

Using merged ozone data, Camp et al. (2003) showed that the QBO is associated with the first EOF mode of tropical TCO, accounting for nearly 42% of the variance. However, the second mode, which accounts for nearly 33% of the variance, is also related to the QBO. The third mode, which accounts for nearly 15% of the variance, represents an interaction between the QBO and an annual cycle. The fourth mode, which accounts for only 3% of the variance, is associated with ENSO. Their result is quite different with shown in this paper, which suggests that the influence of the QBO on ozone is dominated in the first EOF mode. One of the main reasons for the difference between our results and those of Camp et al. (2003) is that this study focuses on lower stratospheric ozone, whereas Camp et al. (2003) analyzed changes in TCO. The change in TCO is dominated by ozone variability in the lower to middle stratosphere, so that the QBO explains more variance than other factors. These findings imply that the contribution of a given factor to stratospheric ozone variation can differ between atmospheric layers.

An EOF analysis using TOMCAT/SLIMCAT simulation data was also performed to confirm the results from the analysis of SWOOSH data. Figure 5 shows the EOF spatial patterns and PCs of lower stratospheric ozone variations based on TOMCAT/SLIMCAT data for 2000–2015 in the range 50°S to 50°N and 100–50 hPa and the possible relevant impact factors of the leading three modes, respectively. Modes 1–3 account for 50.0%, 25.1%, and 13.7% of the variance, respectively. These results are similar

Table 2
The Corresponding SRs Among Figures 4a, 4b, 4c, and 4d

SRs	SST & PC2 (Figure 4c)	SST & PC3 (Figure 4d)
Canonical ENSO-related SST (Figure 4a)	0.78* (0.71, 0.88)	0.42 (0.27, 0.61)
ENSO Modoki-related SST (Figure 4b)	0.43 (0.39, 0.63)	0.69* (0.31, 0.70)

Note. Asterisks indicate that the correlation coefficient is significant at the 95% confidence level. The values in brackets are the uncertainty range for the correlation coefficient at the 95% confidence level. ENSO = El Niño–Southern Oscillation; PC = principal component; SR = spatial correlation coefficient; SST = sea surface temperature.

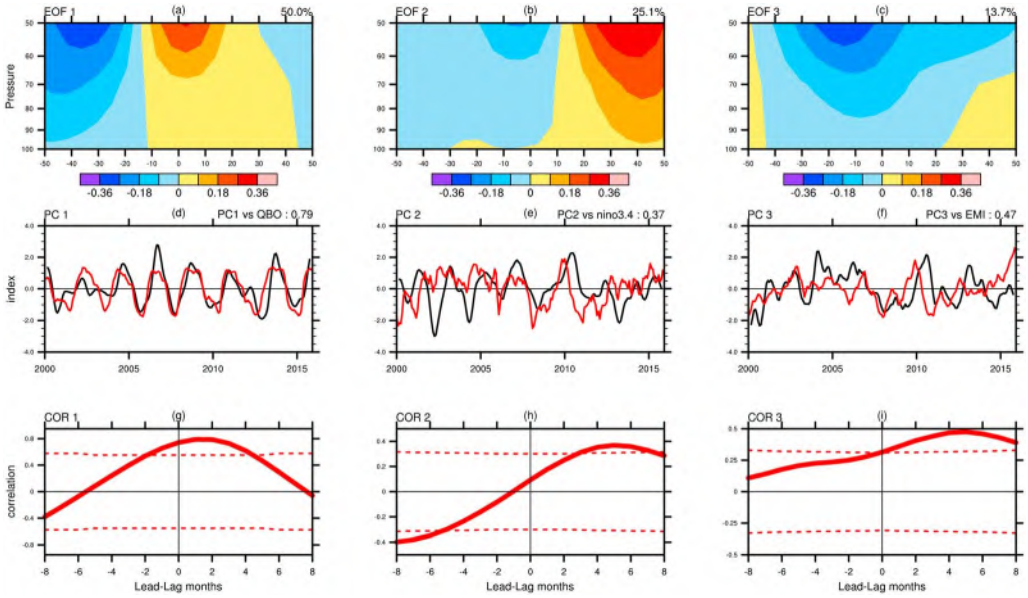

Figure 5. (a, d, and g) As in Figures 1a–1c; (b, e, and h) as in Figures 2a–2c; and (c, f, and i) as in Figures 3a–3c but for ozone anomalies calculated using TOMCAT/SLIMCAT data for 2000–2015. Ozone anomalies were obtained by removing the annual cycle and linear trend from the original time series. EOF = empirical orthogonal function; EMI = El Niño–Southern Oscillation Modoki index; PC = principal component; QBO = quasi-biennial oscillation.

to those obtained using the SWOOSH data. The first mode is related to the QBO (Figures 5a, 5d, and 5g). PC2 is correlated with the NINO3.4 index (Figure 5e, $R = 0.37$), which leads PC2 variations by 4–5 months (Figure 5h). This implies that the second EOF mode is related to canonical ENSO events. The third EOF mode is related to ENSO Modoki; the correlation coefficient between PC3 and the EMI is 0.47 when the EMI leads PC3 by 4–5 months (Figures 5c, 5f, and 5i). Table 3 provides the largest lead-lag correlation coefficients, together with their corresponding uncertainties, between PC1–PC3 and the QBO, canonical ENSO, and ENSO Modoki indices. The values imply that PC1, PC2, and PC3 are associated with the QBO, canonical ENSO, and ENSO Modoki, respectively. These conclusions are consistent with those obtained using observations (Table 1).

The above analyses focus only on lower stratospheric ozone changes during the period 2000–2016. Both EOF analysis based on SWOOSH observations and TOMCAT/SLIMCAT simulation suggest that the first, second, and third modes of ozone changes are related to QBO, canonical ENSO, and ENSO Modoki events, respectively. In order to investigate if the after/before 2000 have different results, we next repeat the analyses but focus on changes prior to 2000. Figures 6a–6c show the EOF spatial patterns of lower stratospheric ozone variations from 1984 to 2000 based on SWOOSH data matching the same latitudes and pressure levels as for the 2000–2016 period. Modes 1–3 account for 30.7%, 25.8%, and 11.7% of the variance, respectively. The first EOF mode (Figure 6a) is similar to that based on SWOOSH data for 2000–2016 (Figure 1a). Regarding the second and third modes, however, there are large discrepancies between the results for the 1984–2000 period and those for the 2000–2016 period. Specifically, in comparing Figures 6b and 6c with Figures 2a and 3a, it is evident that the second and third EOF modes have opposite signs in the two periods. This implies that during 1984–2000 the second EOF mode of lower stratospheric ozone variation was related to ENSO Modoki and the third EOF mode was associated with canonical ENSO. Further analysis suggests that the times series of PC1, PC2, and PC3 are correlated with the QBO, EMI, and NINO3.4 indices, respectively (not shown). Figure 6d shows the distribution

Table 3
As in Table 1 but for TOMCAT/SLIMCAT Model Data for 2000–2015

	QBO	NINO3.4	EMI
PC1	0.79* (0.67, 0.81)	0.16 (−0.08, 0.20)	−0.15 (−0.22, 0.06)
PC2	−0.30* (−0.52, −0.28)	0.37* (−0.04, 0.40)	0.21 (−0.03, 0.25)
PC3	0.28* (0.08, 0.35)	0.27* (0.06, 0.33)	0.47* (0.19, 0.51)

Note. EMI = El Niño–Southern Oscillation Modoki index; PC = principal component; QBO = quasi-biennial oscillation.

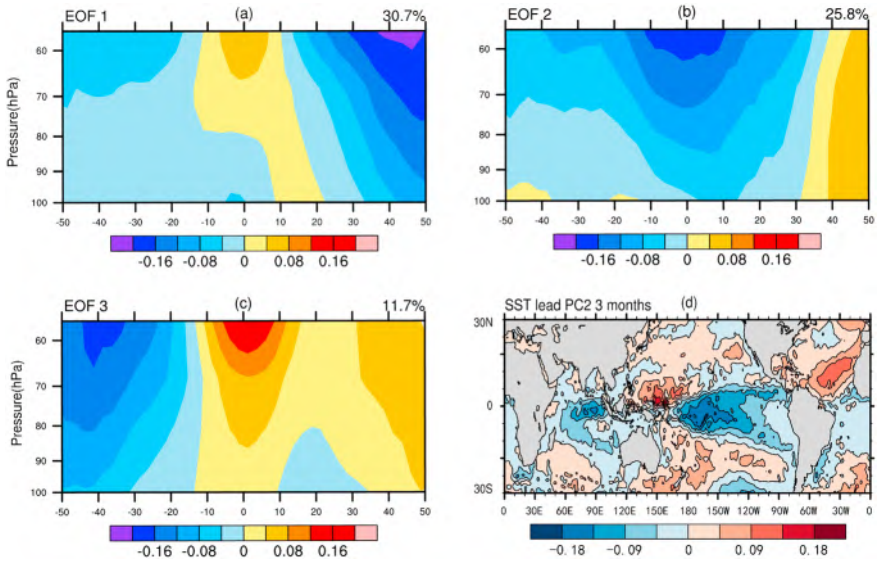

Figure 6. EOF analysis of zonal mean ozone variability for the period 1984–2000 based on Stratospheric Water and Ozone Satellite Homogenized data for 50°S to 50°N and 100–50 hPa. (a–c) Spatial patterns of EOF modes 1–3. (d) Spatial distribution of correlation coefficients between SST and PC2 variations with SST leading PC2 by 3 months. EOF = empirical orthogonal function; PC = principal component; SST = sea surface temperature.

of correlation coefficients between PC2 and variation in SSTAs. The pattern is similar to that of ENSO Modoki SSTAs (Ashok & Yamagata, 2009; Yeh et al., 2009). The explained variance of the second EOF mode (25.8%), which is related to ENSO Modoki, is nearly twice that of the third EOF mode (11.7%), which is related to canonical ENSO.

Figures 7a–7c show the EOF spatial patterns of lower stratospheric ozone variations from 1984 to 2000 based on TOMCAT/SLIMCAT data matching the same latitudes and pressure levels. The first mode accounts for 45.7% of the variance (Figure 7a). The variance of the second and third modes is 22.9% and 12.9%, respectively (Figures 7b and 7c). These results are consistent with the results based on

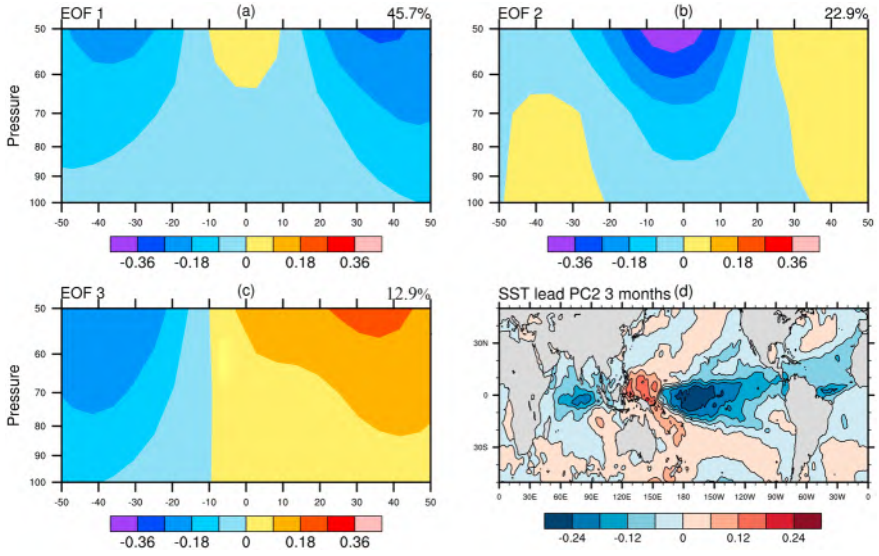

Figure 7. As in Figure 6 but based on TOMCAT/SLIMCAT data. EOF = empirical orthogonal function; PC = principal component; SST = sea surface temperature.

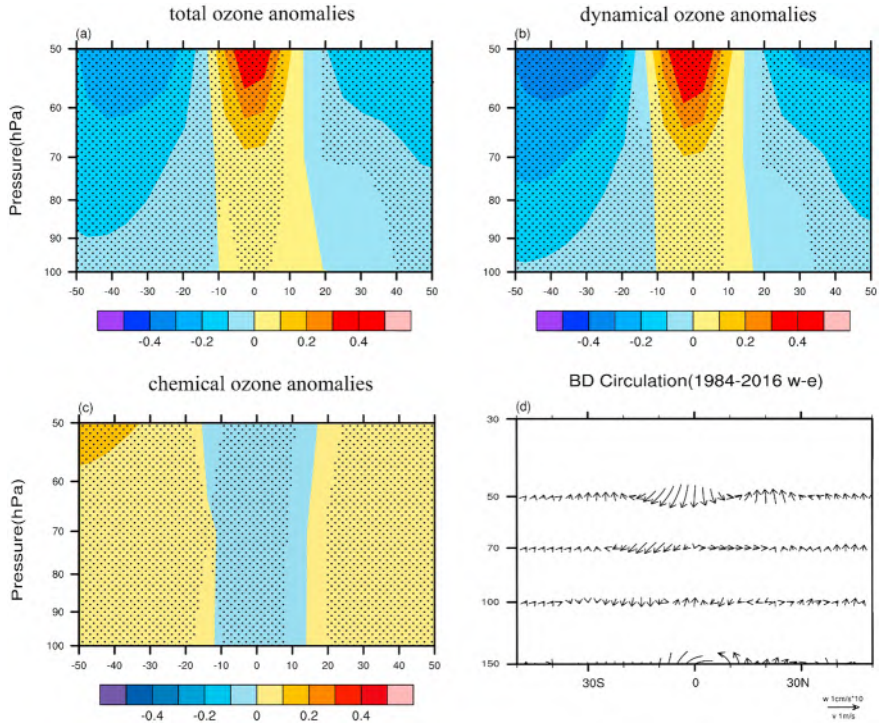

Figure 8. (a) Differences in composite ozone anomalies between the west and east phases (i.e., west phase minus east phase) of quasi-biennial oscillation events (Table 4), based on TOMCAT/SLIMCAT ozone data for 1984–2015. (b) As in (a) but for dynamical ozone. (c) As in (a) but for chemical ozone. (d) As in (a) but for the BD circulation, calculated from the National Centers for Environmental Prediction Reanalysis 2. Canonical ENSO and ENSO Modoki signals were removed from ozone anomaly series by regression analysis before performing the composite analysis. Hatching indicates areas where the correlation coefficients are statistically significant at the 90% confidence level. BD = Brewer-Dobson; ENSO = El Niño–Southern Oscillation.

SWOOSH observations (Figure 6). The spatial distribution of correlation coefficients between PC2 and SST anomaly variation (Figure 7d) is similar to that of ENSO Modoki SSTAs. The results in Figure 7 further confirm that the first, second, and third modes of lower stratospheric ozone variation between 1984 and 2000 correspond to QBO, EMI, and NINO3.4 activity, respectively.

4. Mechanisms by Which the QBO and Two Types of ENSO Affect Interannual Variations in Lower Stratospheric Ozone

The zonal wind anomalies caused by the QBO lead to the dynamical transport of ozone in the middle-upper stratosphere; in addition, a feedback of nitrogen (NO_x) distribution anomalies as a result of the QBO phase can affect ozone via chemical processes in the middle stratosphere (Randel & Wu, 1996; Wallace et al., 1993). ENSO events can significantly influence the BD circulation. For example, enhanced upwelling during El Niño events transports ozone-poor air in the tropics from the troposphere to the stratosphere, which leads to a significant ozone decrease in the lower-middle stratosphere (Camp et al., 2003; Dhomse et al., 2008; Randel et al., 2009; Xie, Li, Tian, Zhang, & Sun, 2014). As a result, the upwelling tends to decrease tropical stratospheric ozone. In addition, the upwelling anomalies can affect ozone by influencing the loss rate in the hydrogen (HO_x) cycle (Meul et al., 2014). For example, increased upwelling reduces the fractional chlorine release from organic source gases by reducing the time available for photolysis.

We now analyze the dynamical and chemical effects of QBO, canonical ENSO, and ENSO Modoki events on lower stratospheric ozone. Figures 8a–8c show the differences in composite ozone anomalies between the west and east phases of QBO events (i.e., west phase minus east phase) during 1984–

Table 4
Easterly Phases (Left Column) and Westerly Phases (Right Column) of Quasi-Biennial Oscillation Events Between 1984 and 2016

Easterly phases (<−5 m/s)	Westerly phases (>5 m/s)
January 1984 to December 1984	March 1985 to April 1986
July 1986 to July 1987	September 1987 to May 1988
May 1989 to February 1990	April 1990 to April 1991
July 1991 to July 1992	November 1992 to June 1993
November 1993 to October 1994	December 1994 to September 1995
January 1996 to December 1996	April 1997 to November 1997
April 1998 to November 1998	February 1999 to December 1999
June 2000 to October 2001	March 2000
April 2003 to December 2003	February 2002 to October 2002
April 2005 to February 2006	March 2004 to October 2004
April 2007 to January 2008	May 2006 to December 2006
June 2009 to July 2010	April 2008 to April 2009
November 2011 to January 2013	September 2010 to May 2011
June 2014 to May 2015	April 2013 to April 2014
	July 2015 to December 2015

2015 (Table 4) and the corresponding dynamic and chemical ozone anomalies derived from TOMCAT/SLIMCAT simulations. Compared with the east QBO, the west QBO causes an increase of ozone in the tropical lower stratosphere but a decrease in the middle latitudes of both hemispheres (Figure 8a). The decrease in the SH is larger than that in the NH. The pattern of ozone anomalies is consistent with the first EOF mode of stratospheric ozone variation (Figure 1a). The pattern of

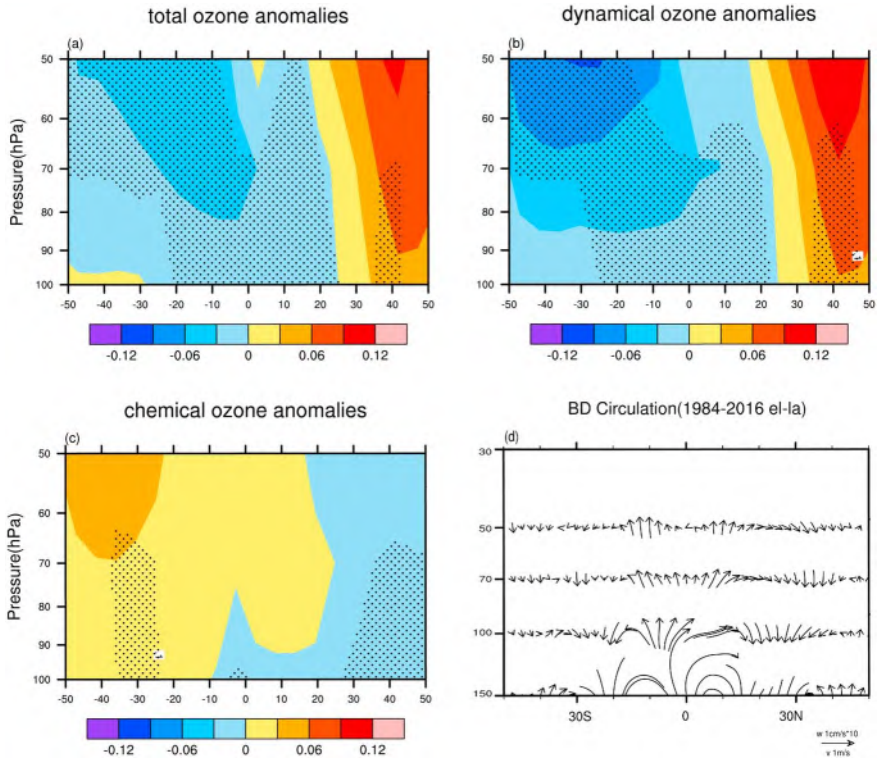

Figure 9. As in Figure 8 but for canonical ENSO events (warm phase minus cold phase). The selected canonical ENSO events are listed in Table 5. Quasi-biennial oscillation and ENSO Modoki signals were removed from ozone anomaly series by regression analysis before performing the composite analysis. BD = Brewer-Dobson; ENSO = El Niño–Southern Oscillation.

Table 5
Canonical El Niño and Canonical La Niña Events During 1984–2000 and 2001–2016

Time (years)	Canonical El Niño	Canonical La Niña
1984–2000	October 1986 to December 1987	May 1988 to April 1989
	June 1997 to April 1998	October 1998 to August 1999
2001–2016	June 2002 to January 2003	September 2007 to March 2008
	August 2006 to January 2007	August 2010 to March 2011
	April 2015 to December 2015	

dynamical ozone anomalies (Figure 8b) is similar to that of total ozone anomalies (Figure 8a), while the pattern of chemical ozone anomalies (Figure 8c) is opposite to that of total ozone anomalies (Figure 8a). This implies that dynamical and chemical processes caused by the QBO have opposite effects on lower stratospheric ozone. In addition, the effect of dynamical processes on total ozone anomalies is 3–4 times greater than the effect of chemical processes. The west phase of the QBO causes anomalous downwelling in the stratosphere in the lower latitudes but anomalous upwelling in the middle latitudes (Figure 8d), resulting in a positive anomaly of ozone in the tropical lower stratosphere but a negative anomaly in the middle latitudes. Chipperfield et al. (1994) demonstrated from model results that the two-cell structure in lower stratospheric ozone is due to the mean vertical transport. However, the decrease of ozone in the tropical lower stratosphere and the increase in the middle latitudes (Figure 8c) are due to reactive nitrogen (NO_y) associated with chemical process in the middle stratosphere (Chipperfield et al., 1994; Randel & Wu, 1996).

Figure 9 shows the differences in composite ozone anomalies between warm and cold phases (i.e., warm phase minus cold phase) of canonical ENSO events from 1984–2015 (Table 5) and the corresponding dynamical and chemical ozone anomalies. The pattern shown in Figure 9a agrees with the corresponding EOF modes (Figure 2a), with negative ozone anomalies in the tropical and SH lower stratosphere and positive ozone anomalies in the NH. Figures 9b and 9c show that dynamic processes dominate changes in lower stratospheric ozone; chemical processes lead to positive ozone anomalies in the tropical and lower stratosphere of the SH but negative ozone anomalies in the middle latitudes of the NH. During El Niño phases of ENSO, enhanced tropical upwelling (Figure 9d) transports more ozone-poor air from the troposphere to the stratosphere (Fueglistaler & Haynes, 2005; Geller et al., 2002; Gettelman et al., 2001; Hatsushika & Yamazaki, 2003; Scaife et al., 2003; Xie, Li, Tian, Zhang, & Shu, 2014). In addition, downwelling anomalies are found in the NH (Figure 9d). The presence of downwelling anomalies explains the increase of ozone in the NH due to changes in the BD circulation. A faster (slower) circulation in general would slow (speed up) ozone destruction cycles caused by NO_x, HO_x, Cl_x, and Br_x catalytic cycles (Tian et al., 2009). This result explains the pattern of chemical ozone anomalies in the lower stratosphere (Figure 9c).

The differences in composite ozone anomalies between warm and cold phases (i.e., warm phase minus cold phase) of ENSO Modoki events from 1984–2015 (Table 6) are shown in Figure 10. The pattern of ozone anomalies (Figure 10a) is similar to the third EOF mode of lower stratospheric ozone variations (Figure 3a). Namely, the negative anomaly of ozone in the stratosphere (Figure 10a) is similar to that

Table 6
El Niño Modoki and La Niña Modoki Events During 1984–2000 and 2001–2016

Time (years)	El Niño Modoki	La Niña Modoki
1984–2000	October 1990 to June 1991	October 1988 to April 1989
	August 1991 to June 1992	March 1998 to May 1999
	June 1994 to May 1995	November 1999 to May 2000
2001–2016	July 2009 to March 2010	January 2008 to September 2008
		August 2010 to April 2011

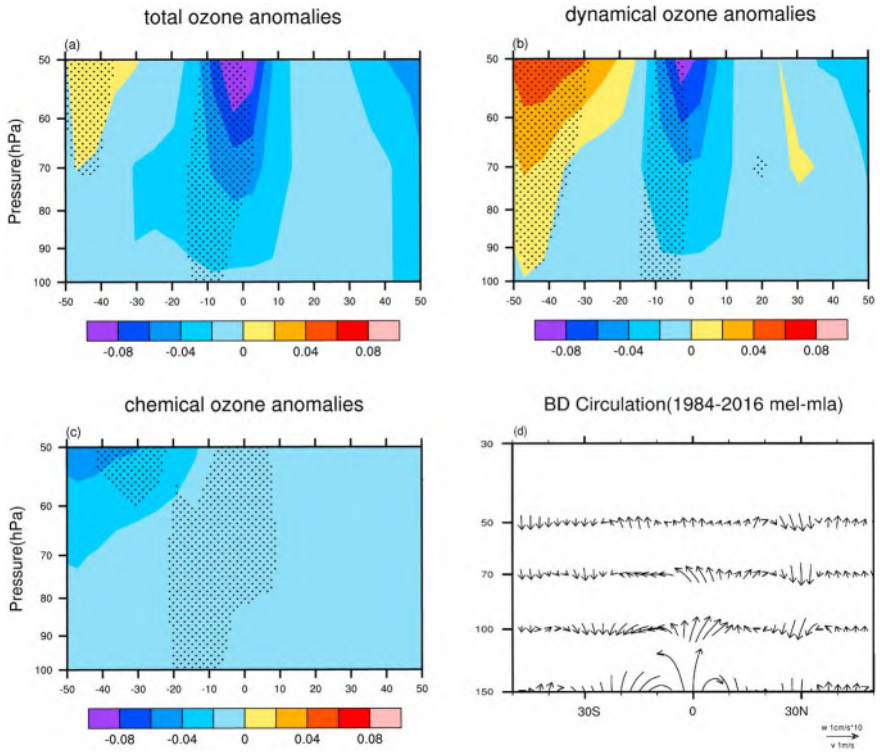

Figure 10. As in Figure 8 but for ENSO Modoki events (warm phase minus cold phase). The selected ENSO Modoki events are listed in Table 6. Canonical ENSO and quasi-biennial oscillation signals were removed from ozone anomaly series by regression analysis before performing the composite analysis. BD = Brewer-Dobson; ENSO = El Niño–Southern Oscillation.

shown in Figure 3a. Figure 10b illustrates that dynamic transport causes stratospheric ozone to increase in the middle and high latitudes of the SH. The ozone decrease in the stratosphere in the middle and high latitudes of the SH is the combined effect of dynamic transport (Figure 10b) and chemical destruction (Figure 10c). The dynamical and chemical ozone anomalies correspond to the enhanced upwelling in the lower latitudes and anomalous downwelling in the middle latitudes of the SH (Figure 10d).

The above analysis poses an interesting question: Why did ENSO Modoki have a greater impact on ozone than canonical ENSO before 2000 and a weaker impact after 2000? The occurrence of canonical ENSO and ENSO Modoki events for the periods 1984–2000 and 2001–2016 are listed in Table 7, and the definitions of the two types of ENSO event follow Yu et al. (2012). There was a high frequency of ENSO Modoki events between 1980 and 2000 (Ashok & Yamagata, 2009; Yeh et al., 2009). After 2000, the frequency of canonical ENSO is higher than that of ENSO Modoki events. These results suggest ENSO Modoki events had a greater impact on lower stratospheric ozone before 2000. Figure 11 shows the differences in composite BD circulation anomalies between warm and cold phases of canonical ENSO and ENSO Modoki events for 1984–2000 and 2001–2016. The BD circulation in the tropical lower stratosphere is stronger during ENSO Modoki events (Figure 11b) than during canonical ENSO events for the period 1984–2000 (Figure 11a), whereas the opposite is true the 2001–2016 period.

Table 7
Canonical El Niño and El Niño Modoki Events During 1984–2000 and 2001–2016

The type of event	1984–2000	2001–2016
Canonical El Niño	1986/1987	2002/2003
	1997/1998	2006/2007
		2015/2016
El Niño Modoki	1990/1991	2009/2010
	1991/1992	
	1994/1995	

Note. The definitions of the two types of El Niño–Southern Oscillation event follow Yu et al. (2012).

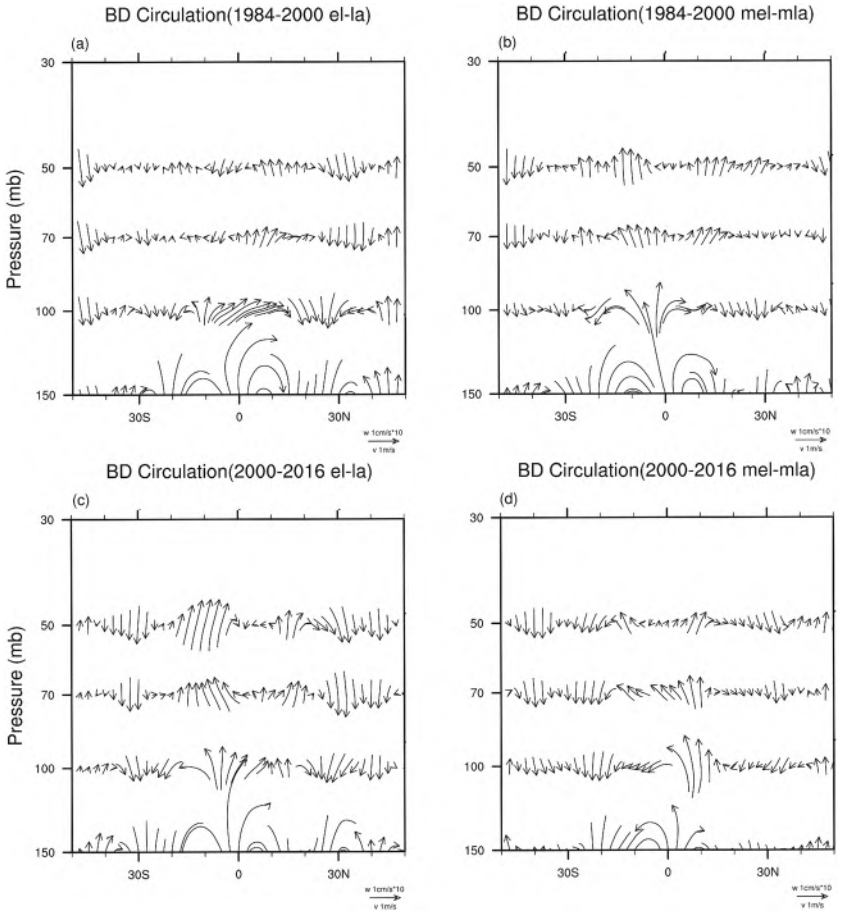

Figure 11. (a) Differences in BD circulation anomalies between warm and cold phases of (a) canonical ENSO and (b) ENSO Modoki events for 1984–2000. (c, d) As in (a) and (b) but for the 2000–2016 period. BD = Brewer-Dobson; ENSO = El Niño–Southern Oscillation.

5. Conclusions

We investigated interannual variations in lower stratospheric ozone from 1984 to 2016 using SWOOSH observational data and TOMCAT/SLIMCAT model simulation data. Based on EOF analysis of lower stratospheric ozone from 2000 to 2016, we find that the first three EOFs capture nearly 80% of the variance. The first, second, and third modes are related to QBO, canonical ENSO, and ENSO Modoki events, respectively. During 1984–2000 the first mode is also related the QBO. However, unlike the 2000–2016 period, the second mode is related to ENSO Modoki and the third mode to canonical ENSO events. Furthermore, during the 1984–2000 period the explained variance of the second mode is twice that of the third mode. Since the frequency of ENSO Modoki events was higher than that of canonical ENSO between 1984 and 2000, the BD circulation anomalies related to ENSO Modoki were stronger than those related to canonical ENSO. This led to ENSO Modoki events having a greater impact on lower stratospheric ozone before 2000 than after.

The influences of dynamic processes and chemical processes related to QBO, canonical ENSO, and ENSO Modoki events on lower stratospheric ozone were also analyzed. Dynamical processes related to the west phase of the QBO cause an increase in ozone in the tropical lower stratosphere but a decrease in the middle latitudes of both hemispheres, while chemical processes related to the west QBO phase have the opposite impact on ozone. In contrast, the effect of dynamical ozone is 3–4 times greater than that of chemical ozone. Dynamical processes related to the warm phase of canonical ENSO events cause negative ozone anomalies in the tropical and the SH lower stratosphere and an increase in the NH, while chemical processes related to warm canonical ENSO events lead to negative ozone anomalies in the tropical and SH lower stratosphere

but a weak impact on NH lower stratospheric ozone. Dynamical processes related to the warm phase of ENSO Modoki increase ozone in the middle latitude stratosphere of the SH but decrease ozone in the lower latitude stratosphere, due to the combined effect of dynamic transport and chemical destruction.

Although factors that drive interannual changes in ozone have been extensively analyzed in the past, it is known that these contributions vary over time. Therefore, we analyzed interannual changes in lower stratospheric ozone over the past 30 years. We find that as the strength of canonical ENSO and ENSO Modoki events varies over time, their relative contributions to ozone variation also vary. Therefore, predicting future changes in ENSO will benefit the prediction of future changes in lower stratospheric ozone. It has been suggested that in the context of continued global warming, both types of ENSO event might become stronger and more frequent. Future studies should consider whether the contribution of ENSO activities to variation in lower stratospheric ozone is likely to continue to increase in the future and whether it will eventually exceed that of the QBO.

Acknowledgments
Funding for this work was provided by the SOA International Cooperation Program on Global Change and Air–Sea Interactions (GASI-IPOVAI-03) and the National Natural Science Foundation of China (41630421). We acknowledge ozone data sets from the SWOOSH (The SWOOSH data can be accessed at https://www.esrl.noaa.gov/csd/groups/csd8/swoosh; Davis et al., 2016), meteorological fields from NCEP2, and sea surface temperature from the Hadley Centre. The results of TOMCAT/SLIMCAT output can be accessed at https://zenodo.org/record/2652838#.XMRgxvZuLmQ, and the original data are available from Wuhu Feng (w.feng@ncas.ac.uk) on reasonable request. We thank ECMWF for providing the ERA-Interim analyses that are archived on ECMWF MARS (Meteorological Archival and Retrieval System).

References

Ashok, K., Behera, S. K., Rao, S. A., Weng, H., & Yamagata, T. (2007). El Niño Modoki and its possible teleconnection. *Journal of Geophysical Research*, *112*, C11007. https://doi.org/10.1029/2006JC003798

Ashok, K., & Yamagata, T. (2009). Climate change: The El Niño with a difference. *Nature*, *461*(7263), 481–484. https://doi.org/10.1038/461481a

Baldwin, M. P., & Dunkerton, T. J. (2001). Stratospheric harbingers of anomalous weather regimes. *Science*, *294*(5542), 581–584. https://doi.org/10.1126/science.1063315

Ball, W. T., Alsing, J., Mortlock, D. J., Rozanov, E. V., Tummon, F., & Haigh, J. D. (2017). Reconciling differences in stratospheric ozone composites. *Atmospheric Chemistry and Physics*, *17*(20), 12,269–12,302. https://doi.org/10.5194/acp-17-12269-2017

Ball, W. T., Alsing, J., Mortlock, D. J., Staehelin, J., Haigh, J. D., Peter, T., et al. (2018). Evidence for a continuous decline in lower stratospheric ozone offsetting ozone layer recovery. *Atmospheric Chemistry and Physics*, *18*(2), 1379–1394. https://doi.org/10.5194/acp-18-1379-2018

Bretherton, C. S., Widmann, M., Dymnikov, V. P., Wallace, J. M., & Bladé, I. (1999). The effective number of spatial degrees of freedom of a time-varying field. *Journal of Climate*, *12*(7), 1990–2009. https://doi.org/10.1175/1520-0442(1999)012<1990:TENOSD>2.0.CO;2

Brewer, A. (1949). Evidence for a world circulation provided by the measurements of helium and water vapour distribution in the stratosphere. *Quarterly Journal of the Royal Meteorological Society*, *75*(326), 351–363. https://doi.org/10.1002/qj.49707532603

Brönnimann, S., Luterbacher, J., Staehelin, J., Svendby, T., Hansen, G., & Svenøe, T. (2004). Extreme climate of the global troposphere and stratosphere in 1940–42 related to El Niño. *Nature*, *431*(7011), 971–974. https://doi.org/10.1038/nature02982

Brönnimann, S., Schraner, M., Müller, B., Fischer, A., Brunner, D., Rozanov, E., & Egorova, T. (2006). The 1986–1989 ENSO cycle in a chemical climate model. *Atmospheric Chemistry and Physics*, *6*(12), 4669–4685. https://doi.org/10.5194/acp-6-4669-2006

Butchart, N., Scaife, A. A., Austin, J., Hare, S. H., & Knight, J. R. (2003). Quasi-biennial oscillation in ozone in a coupled chemistry-climate model. *Journal of Geophysical Research*, *108*(D15), 4486. https://doi.org/10.1029/2002JD003004

Cagnazzo, C., Manzini, E., Calvo, N., Douglass, A., Akiyoshi, H., Bekki, S., et al. (2009). Northern winter stratospheric temperature and ozone responses to ENSO inferred from an ensemble of Chemistry Climate Models. *Atmospheric Chemistry and Physics*, *9*(22), 8935–8948. https://doi.org/10.5194/acp-9-8935-2009

Calvo, N., Garcia, R., Randel, W., & Marsh, D. (2010). Dynamical mechanism for the increase in tropical upwelling in the lowermost tropical stratosphere during warm ENSO events. *Journal of the Atmospheric Sciences*, *67*(7), 2331–2340. https://doi.org/10.1175/2010JAS3433.1

Camp, C., & Tung, K. K. (2007). Stratospheric polar warming by ENSO in winter: A statistical study. *Geophysical Research Letters*, *34*, L04809. https://doi.org/10.1029/2006GL028521

Camp, C. D., Roulston, M. S., & Yung, Y. L. (2003). Temporal and spatial patterns of the interannual variability of total ozone in the tropics. *Journal of Geophysical Research*, *108*(D20), 4643. https://doi.org/10.1029/2001JD001504

Chipperfield, M. (2006). New version of the TOMCAT/SLIMCAT off-line chemical transport model: Intercomparison of stratospheric tracer experiments. *Quarterly Journal of the Royal Meteorological Society*, *132*(617), 1179–1203. https://doi.org/10.1256/qj.05.51

Chipperfield, M., Gray, L., Kinnersley, J., & Zawodny, J. (1994). A two-dimensional model study of the QBO signal in SAGE II NO_2 and O_3. *Geophysical Research Letters*, *21*(7), 589–592. https://doi.org/10.1029/94GL00211

Chipperfield, M. P., Dhomse, S., Hossaini, R., Feng, W., Santee, M. L., Weber, M., et al. (2018). On the cause of recent variations in lower stratospheric ozone. *Geophysical Research Letters*, *45*, 5718–5726. https://doi.org/10.1029/2018GL078071

Davis, S. M., Rosenlof, K. H., Hassler, B., Hurst, D. F., Read, W. G., Vömel, H., et al. (2016). The Stratospheric Water and Ozone Satellite Homogenized (SWOOSH) database: A long-term database for climate studies. *Earth System Science Data*, *8*(2), 461–490. https://doi.org/10.5194/essd-8-461-2016

Dee, D. P., Uppala, S. M., Simmons, A., Berrisford, P., Poli, P., Kobayashi, S., et al. (2011). The ERA-Interim reanalysis: Configuration and performance of the data assimilation system. *Quarterly Journal of the Royal Meteorological Society*, *137*(656), 553–597. https://doi.org/10.1002/qj.828

Dhomse, S., Weber, M., & Burrows, J. (2008). The relationship between tropospheric wave forcing and tropical lower stratospheric water vapor. *Atmospheric Chemistry and Physics*, *8*(3), 471–480. https://doi.org/10.5194/acp-8-471-2008

Edmon, H. Jr., Hoskins, B., & McIntyre, M. (1980). Eliassen-Palm cross sections for the troposphere. *Journal of the Atmospheric Sciences*, *37*(12), 2600–2616. https://doi.org/10.1175/1520-0469(1980)037<2600:EPCSFT>2.0.CO;2

Feng, W., Chipperfield, M., Davies, S., Mann, G., Carslaw, K., Dhomse, S., et al. (2011). Modelling the effect of denitrification on polar ozone depletion for Arctic winter 2004/2005. *Atmospheric Chemistry and Physics*, *11*(13), 6559–6573. https://doi.org/10.5194/acp-11-6559-2011

Feng, W., Chipperfield, M., Davies, S., von der Gathen, P., Kyrö, E., Volk, C., et al. (2007). Large chemical ozone loss in 2004/2005 Arctic winter/spring. *Geophysical Research Letters*, *34*, L09803. https://doi.org/10.1029/2006GL029098

Feng, W., Chipperfield, M., Roscoe, H., Remedios, J., Waterfall, A., Stiller, G., et al. (2005). Three-dimensional model study of the Antarctic ozone hole in 2002 and comparison with 2000. *Journal of the Atmospheric Sciences*, *62*(3), 822–837. https://doi.org/10.1175/JAS-3335.1

Forster, F., Piers, M., & Shine, K. P. (1997). Radiative forcing and temperature trends from stratospheric ozone changes. *Journal of Geophysical Research*, *102*(D9), 10,841–10,855. https://doi.org/10.1029/96JD03510

Free, M., & Seidel, D. J. (2009). Observed El Niño–Southern Oscillation temperature signal in the stratosphere. *Journal of Geophysical Research*, *114*, D23108. https://doi.org/10.1029/2009JD012420

Fueglistaler, S., & Haynes, P. (2005). Control of interannual and longer-term variability of stratospheric water vapor. *Journal of Geophysical Research*, *110*, D24108. https://doi.org/10.1029/2005JD006019

Fusco, A. C., & Salby, M. L. (1999). Interannual variations of total ozone and their relationship to variations of planetary wave activity. *Journal of Climate*, *12*(6), 1619–1629. https://doi.org/10.1175/1520-0442(1999)012<1619:IVOTOA>2.0.CO;2

Garcia-Herrera, R., Calvo, N., Garcia, R., & Giorgetta, M. (2006). Propagation of ENSO temperature signals into the middle atmosphere: A comparison of two general circulation models and ERA-40 reanalysis data. *Journal of Geophysical Research*, *111*, D06101. https://doi.org/10.1029/2005JD006061

Garfinkel, C., & Hartmann, D. (2007). Effects of the El Niño–Southern Oscillation and the quasi-biennial oscillation on polar temperatures in the stratosphere. *Journal of Geophysical Research*, *112*, D19112. https://doi.org/10.1029/2007JD008481

Garfinkel, C., & Hartmann, D. (2008). Different ENSO teleconnections and their effects on the stratospheric polar vortex. *Journal of Geophysical Research*, *113*, D18114. https://doi.org/10.1029/2008JD009920

Garfinkel, C., Hurwitz, M., Waugh, D., & Butler, A. (2013). Are the teleconnections of Central Pacific and Eastern Pacific El Niño distinct in boreal wintertime? *Climate Dynamics*, *41*(7-8), 1835–1852. https://doi.org/10.1007/s00382-012-1570-2

Gebhardt, C., Rozanov, A., Hommel, R., Weber, M., Bovensmann, H., Burrows, J., et al. (2014). Stratospheric ozone trends and variability as seen by SCIAMACHY from 2002 to 2012. *Atmospheric Chemistry and Physics*, *14*(2), 831–846. https://doi.org/10.5194/acp-14-831-2014

Geller, M. A., Zhou, X., & Zhang, M. (2002). Simulations of the interannual variability of stratospheric water vapor. *Journal of the Atmospheric Sciences*, *59*(6), 1076–1085. https://doi.org/10.1175/1520-0469(2002)059<1076:SOTIVO>2.0.CO;2

Gettelman, A., Randel, W., Massie, S., Wu, F., Read, W. G., & Russell, J. III (2001). El Nino as a natural experiment for studying the tropical tropopause region. *Journal of Climate*, *14*(16), 3375–3392. https://doi.org/10.1175/1520-0442(2001)014<3375:ENOAAN>2.0.CO;2

Graf, H. F., & Walter, K. (2005). Polar vortex controls coupling of North Atlantic Ocean and atmosphere. *Geophysical Research Letters*, *32*, , L01704. https://doi.org/10.1029/2004GL020664

Haigh, J. D. (1994). The role of stratospheric ozone in modulating the solar radiative forcing of climate. *Nature*, *370*(6490), 544–546. https://doi.org/10.1038/370544a0

Hamilton, K. (1995). Interannual variability in the Northern Hemisphere winter middle atmosphere in control and perturbed experiments with the GFDL SKYHI general circulation model. *Journal of the Atmospheric Sciences*, *52*(1), 44–66. https://doi.org/10.1175/1520-0469(1995)052<0044:IVITNH>2.0.CO;2

Hatsushika, H., & Yamazaki, K. (2003). Stratospheric drain over Indonesia and dehydration within the tropical tropopause layer diagnosed by air parcel trajectories. *Journal of Geophysical Research*, *108*(D19), 4610. https://doi.org/10.1029/2002JD002986

Hegyi, B. M., & Deng, Y. (2011). A dynamical fingerprint of tropical Pacific sea surface temperatures on the decadal-scale variability of cool-season Arctic precipitation. *Journal of Geophysical Research*, *116*, D20121. https://doi.org/10.1029/2011JD016001

Hu, D., Tian, W., Xie, F., Wang, C., & Zhang, J. (2015). Impacts of stratospheric ozone depletion and recovery on wave propagation in the boreal winter stratosphere. *Journal of Geophysical Research: Atmospheres*, *120*, 8299–8317. https://doi.org/10.1002/2014JD022855

Hurwitz, M., Newman, P., Oman, L., & Molod, A. (2011). Response of the Antarctic stratosphere to two types of El Niño events. *Journal of the Atmospheric Sciences*, *68*(4), 812–822. https://doi.org/10.1175/2011JAS3606.1

Hurwitz, M. M., Song, I.-S., Oman, L. D., Newman, P. A., Molod, A. M., Frith, S. M., & Nielsen, J. E. (2011). Response of the Antarctic stratosphere to warm pool El Niño events in the GEOS CCM. *Atmospheric Chemistry and Physics*, *11*(18), 9659–9669. https://doi.org/10.5194/acp-11-9659-2011

Ineson, S., & Scaife, A. (2009). The role of the stratosphere in the European climate response to El Niño. *Nature Geoscience*, *2*(1), 32–36. https://doi.org/10.1038/ngeo381

Iza, M., & Calvo, N. (2015). Role of stratospheric sudden warmings on the response to central Pacific El Niño. *Geophysical Research Letters*, *42*, 2482–2489. https://doi.org/10.1002/2014GL062935

Iza, M., Calvo, N., & Manzini, E. (2016). The stratospheric pathway of La Niña. *Journal of Climate*, *29*(24), 8899–8914. https://doi.org/10.1175/JCLI-D-16-0230.1

Karpechko, A. Y., Perlwitz, J., & Manzini, E. (2014). A model study of tropospheric impacts of the Arctic ozone depletion 2011. *Journal of Geophysical Research: Atmospheres*, *119*, 7999–8014. https://doi.org/10.1002/2013JD021350

Kerr, J., & McElroy, C. (1993). Evidence for large upward trends of ultraviolet-B radiation linked to ozone depletion. *Science*, *262*(5136), 1032–1034. https://doi.org/10.1126/science.262.5136.1032

Kidston, J., Scaife, A. A., Hardiman, S. C., Mitchell, D. M., Butchart, N., Baldwin, M. P., & Gray, L. J. (2015). Stratospheric influence on tropospheric jet streams, storm tracks and surface weather. *Nature Geoscience*, *8*(6), 433–440. https://doi.org/10.1038/ngeo2424

Kyrölä, E., Laine, M., Sofieva, V., Tamminen, J., Päivärinta, S.-M., Tukiainen, S., et al. (2013). Combined SAGE II–GOMOS ozone profile data set for 1984–2011 and trend analysis of the vertical distribution of ozone. *Atmospheric Chemistry and Physics*, *13*(21), 10,645–10,658. https://doi.org/10.5194/acp-13-10645-2013

Lee, S., Shelow, D., Thompson, A., & Miller, S. (2010). QBO and ENSO variability in temperature and ozone from SHADOZ, 1998–2005. *Journal of Geophysical Research*, *115*, D18105. https://doi.org/10.1029/2009JD013320

Li, T., Calvo, N., Yue, J., Russell, J. M. III, Smith, A. K., Mlynczak, M. G., et al. (2016). Southern Hemisphere summer mesopause responses to El Niño–Southern Oscillation. *Journal of Climate*, *29*(17), 6319–6328. https://doi.org/10.1175/JCLI-D-15-0816.1

Lindsay, R., Wensnahan, M., Schweiger, A., & Zhang, J. (2014). Evaluation of seven different atmospheric reanalysis products in the Arctic. *Journal of Climate*, *27*(7), 2588–2606. https://doi.org/10.1175/JCLI-D-13-00014.1

Lubin, D., & Jensen, E. H. (1995). Effects of clouds and stratospheric ozone depletion on ultraviolet radiation trends. *Nature*, *377*(6551), 710–713. https://doi.org/10.1038/377710a0

Manzini, E., Giorgetta, M., Esch, M., Kornblueh, L., & Roeckner, E. (2006). The influence of sea surface temperatures on the northern winter stratosphere: Ensemble simulations with the MAECHAM5 model. *Journal of Climate*, *19*(16), 3863–3881. https://doi.org/10.1175/JCLI3826.1

Meul, S., Langematz, U., Oberländer, S., Garny, H., & Jöckel, P. (2014). Chemical contribution to future tropical ozone change in the lower stratosphere. *Atmospheric Chemistry and Physics*, *14*(6), 2959–2971. https://doi.org/10.5194/acp-14-2959-2014

Mitchell, D., Gray, L., & Charlton-Perez, A. (2011). The structure and evolution of the stratospheric vortex in response to natural forcings. *Journal of Geophysical Research*, *116*, D15110. https://doi.org/10.1029/2011JD015788

Nair, P., Froidevaux, L., Kuttippurath, J., Zawodny, J., Russell, J., Steinbrecht, W., et al. (2015). Subtropical and midlatitude ozone trends in the stratosphere: Implications for recovery. *Journal of Geophysical Research: Atmospheres*, *120*, 7247–7257. https://doi.org/10.1002/2014JD022371

Polvani, L. M., Sun, L., Butler, A. H., Richter, J. H., & Deser, C. (2017). Distinguishing stratospheric sudden warmings from ENSO as key drivers of wintertime climate variability over the North Atlantic and Eurasia. *Journal of Climate*, *30*(6), 1959–1969. https://doi.org/10.1175/JCLI-D-16-0277.1

Prather, M. J. (1986). Numerical advection by conservation of second-order moments. *Journal of Geophysical Research*, *91*(D6), 6671–6681. https://doi.org/10.1029/JD091iD06p06671

Ramaswamy, V., Schwarzkopf, M., & Randel, W. (1996). Fingerprint of ozone depletion in the spatial and temporal pattern of recent lower-stratospheric cooling. *Nature*, *382*(6592), 616–618. https://doi.org/10.1038/382616a0

Randel, W. J., Garcia, R. R., Calvo, N., & Marsh, D. (2009). ENSO influence on zonal mean temperature and ozone in the tropical lower stratosphere. *Geophysical Research Letters*, *36*, L15822. https://doi.org/10.1029/2009GL039343

Randel, W. J., & Wu, F. (1996). Isolation of the ozone QBO in SAGE II data by singular-value decomposition. *Journal of the Atmospheric Sciences*, *53*(17), 2546–2559. https://doi.org/10.1175/1520-0469(1996)053<2546:IOTOQI>2.0.CO;2

Rao, J., & Ren, R. (2016). Asymmetry and nonlinearity of the influence of ENSO on the northern winter stratosphere: 2. Model study with WACCM. *Journal of Geophysical Research: Atmospheres*, *121*, 9017–9032. https://doi.org/10.1002/2015JD024521

Reed, R. (1964). A tentative model of the 26-month oscillation in tropical latitudes. *Quarterly Journal of the Royal Meteorological Society*, *90*(386), 441–466. https://doi.org/10.1002/qj.49709038607

Reichler, T., Kim, J., Manzini, E., & Kröger, J. (2012). A stratospheric connection to Atlantic climate variability. *Nature Geoscience*, *5*(11), 783–787. https://doi.org/10.1038/ngeo1586

Ren, R.-C., Cai, M., Xiang, C., & Wu, G. (2012). Observational evidence of the delayed response of stratospheric polar vortex variability to ENSO SST anomalies. *Climate Dynamics*, *38*(7-8), 1345–1358. https://doi.org/10.1007/s00382-011-1137-7

Rienecker, M. M., Suarez, M. J., Gelaro, R., Todling, R., Bacmeister, J., Liu, E., et al. (2011). MERRA: NASA's modern-era retrospective analysis for research and applications. *Journal of Climate*, *24*(14), 3624–3648. https://doi.org/10.1175/JCLI-D-11-00015.1

Sassi, F., Kinnison, D., Boville, B., Garcia, R., & Roble, R. (2004). Effect of El Niño–Southern Oscillation on the dynamical, thermal, and chemical structure of the middle atmosphere. *Journal of Geophysical Research*, *109*, D17108. https://doi.org/10.1029/2003JD004434

Scaife, A. A., Butchart, N., Jackson, D. R., & Swinbank, R. (2003). Can changes in ENSO activity help to explain increasing stratospheric water vapor? *Geophysical Research Letters*, *30*(17), 1880. https://doi.org/10.1029/2003GL017591

Sioris, C., McLinden, C., Fioletov, V., Adams, C., Zawodny, J., Bourassa, A., et al. (2014). Trend and variability in ozone in the tropical lower stratosphere over 2.5 solar cycles observed by SAGE II and OSIRIS. *Atmospheric Chemistry and Physics*, *14*(7), 3479–3496. https://doi.org/10.5194/acp-14-3479-2014

Son, S. W., Polvani, L. M., Waugh, D. W., Akiyoshi, H., Garcia, R., Kinnison, D., et al. (2008). The impact of stratospheric ozone recovery on the Southern Hemisphere westerly jet. *Science*, *320*(5882), 1486–1489. https://doi.org/10.1126/science.1155939

Sung, M.-K., Kim, B.-M., & An, S.-I. (2014). Altered atmospheric responses to eastern Pacific and central Pacific El Niños over the North Atlantic region due to stratospheric interference. *Climate Dynamics*, *42*(1-2), 159–170. https://doi.org/10.1007/s00382-012-1661-0

Taguchi, M., & Hartmann, D. L. (2006). Increased occurrence of stratospheric sudden warmings during El Niño as simulated by WACCM. *Journal of Climate*, *19*(3), 324–332. https://doi.org/10.1175/JCLI3655.1

Thompson, D. W., Solomon, S., Kushner, P. J., England, M. H., Grise, K. M., & Karoly, D. J. (2011). Signatures of the Antarctic ozone hole in Southern Hemisphere surface climate change. *Nature Geoscience*, *4*(11), 741–749. https://doi.org/10.1038/ngeo1296

Tian, W., Chipperfield, M. P., Gray, L. J., & Zawodny, J. M. (2006). Quasi-biennial oscillation and tracer distributions in a coupled chemistry-climate model. *Journal of Geophysical Research*, *111*, D20301. https://doi.org/10.1029/2005JD006871

Tian, W., Chipperfield, M. P., & Lü, D. (2009). Impact of increasing stratospheric water vapor on ozone depletion and temperature change. *Advances in Atmospheric Sciences*, *26*(3), 423–437. https://doi.org/10.1007/s00376-009-0423-3

Tian, W., Chipperfield, M. P., Stevenson, D. S., Damoah, R., Dhomse, S., Dudhia, A., et al. (2010). Effects of stratosphere-troposphere chemistry coupling on tropospheric ozone. *Journal of Geophysical Research*, *115*, D00M04. https://doi.org/10.1029/2009JD013515

Van Loon, H., & Labitzke, K. (1987). The Southern Oscillation. Part V: The anomalies in the lower stratosphere of the Northern Hemisphere in winter and a comparison with the quasi-biennial oscillation. *Monthly Weather Review*, *115*(2), 357–369. https://doi.org/10.1175/1520-0493(1987)115<0357:TSOPVT>2.0.CO;2

Vigouroux, C., Blumenstock, T., Coffey, M., Errera, Q., García, O., Jones, N. B., et al. (2015). Trends of ozone total columns and vertical distribution from FTIR observations at eight NDACC stations around the globe. *Atmospheric Chemistry and Physics*, *15*(6), 2915–2933. https://doi.org/10.5194/acp-15-2915-2015

Wallace, J. M., Panetta, R. L., & Estberg, J. (1993). Representation of the equatorial stratospheric quasi-biennial oscillation in EOF phase space. *Journal of the Atmospheric Sciences*, *50*(12), 1751–1762. https://doi.org/10.1175/1520-0469(1993)050<1751:ROTESQ>2.0.CO;2

Wang, L., Kushner, P. J., & Waugh, D. W. (2013). Southern Hemisphere stationary wave response to changes of ozone and greenhouse gases. *Journal of Climate*, *26*(24), 10,205–10,217. https://doi.org/10.1175/JCLI-D-13-00160.1

Wang, W., Matthes, K., Tian, W., Park, W., Shangguan, M., & Ding, A. (2018). Solar impacts on decadal variability of tropopause temperature and lower stratospheric (LS) water vapour: A mechanism through ocean–atmosphere coupling. *Climate Dynamics*, *52*(9-10), 5585–5604.

Wei, K., Chen, W., & Huang, R. (2007). Association of tropical Pacific sea surface temperatures with the stratospheric Holton-Tan Oscillation in the Northern Hemisphere winter. *Geophysical Research Letters*, *34*, L16814. https://doi.org/10.1029/2007GL030478

WMO (World Meteorological Organization), Scientific Assessment of Ozone Depletion: 2018, Global Ozone Research and Monitoring Project–Report No. 58, 588 pp., Geneva, Switzerland, 2018.

Xie, F., Li, J., Tian, W., Feng, J., & Huo, Y. (2012). Signals of El Niño Modoki in the tropical tropopause layer and stratosphere. *Atmospheric Chemistry and Physics*, *12*(11), 5259–5273. https://doi.org/10.5194/acp-12-5259-2012

Xie, F., Li, J., Tian, W., Fu, Q., Jin, F.-F., Hu, Y., et al. (2016). A connection from Arctic stratospheric ozone to El Niño-Southern oscillation. *Environmental Research Letters*, *11*(12). https://doi.org/10.1088/1748-9326/11/12/124026

Xie, F., Li, J., Tian, W., Zhang, J., & Shu, J. (2014). The impacts of two types of El Niño on global ozone variations in the last three decades. *Advances in Atmospheric Sciences*, *31*(5), 1113–1126. https://doi.org/10.1007/s00376-013-3166-0

Xie, F., Li, J., Tian, W., Zhang, J., & Sun, C. (2014). The relative impacts of El Niño Modoki, canonical El Niño, and QBO on tropical ozone changes since the 1980s. *Environmental Research Letters*, *9*(6), 064020. https://doi.org/10.1088/1748-9326/9/6/064020

Yeh, S.-W., Kug, J.-S., Dewitte, B., Kwon, M.-H., Kirtman, B. P., & Jin, F.-F. (2009). El Niño in a changing climate. *Nature*, *461*(7263), 511–514. https://doi.org/10.1038/nature08316

Yu, J. Y., Zou, Y., Kim, S. T., & Lee, T. (2012). The changing impact of El Niño on US winter temperatures. *Geophysical Research Letters*, *39*, L15702. https://doi.org/10.1029/2012GL052483

Zhang, J., Tian, W., Chipperfield, M. P., Xie, F., & Huang, J. (2016). Persistent shift of the Arctic polar vortex towards the Eurasian continent in recent decades. *Nature Climate Change*, *6*(12), 1094–1099. https://doi.org/10.1038/nclimate3136

Zhang, J., Tian, W., Wang, Z., Xie, F., & Wang, F. (2015). The influence of ENSO on northern midlatitude ozone during the winter to spring transition. *Journal of Climate*, *28*(12), 4774–4793. https://doi.org/10.1175/JCLI-D-14-00615.1

Zhang, J., Tian, W., Xie, F., Chipperfield, M. P., Feng, W., Son, S.-W., et al. (2018). Stratospheric ozone loss over the Eurasian continent induced by the polar vortex shift. *Nature communications*, *9*(1), 206. https://doi.org/10.1038/s41467-017-02565-2

Zubiaurre, I., & Calvo, N. (2012). The El Niño–Southern Oscillation (ENSO) Modoki signal in the stratosphere. *Journal of Geophysical Research*, *117*, D04104. https://doi.org/10.1029/2011JD016690